Charge in non-thunderstorm clouds and fogs

Charge in non-thunderstorm clouds and fogs

Charge in non-thunderstorm clouds and fogs

R Giles Harrison, Keri A Nicoll, Maarten HP Ambaum

Department of Meteorology, University of Reading, Reading, UK.

r.g.harrison@reading.ac.uk

Abstract. The global atmospheric electric circuit links charge separation in thunderclouds with current flow throughout the atmosphere. This current flow causes charge accumulation on the upper and lower boundaries of clouds and fogs. Thunderclouds are therefore not the only charged clouds in the atmosphere, and other forms of clouds, especially extensive horizontal layer clouds (stratus) are much more abundant globally. To investigate possible effects of charging of natural droplets in clouds, experiments have been undertaken using corona ion emission into fogs, releasing from within and above the fog. During the corona ion release the droplet size distribution was modified, with an increase in small drops. Further, when the ions were released over the fog, the reflectivity of the fog increased by ~2%, about 30s later.

1. Introduction

There is a long history of research into charge and its effects in the lower atmosphere[1]. Improving understanding of thunderclouds was probably the fundamental original motivation, and related investigations rapidly found that charge occurred in many other atmospheric circumstances, including non-thunderstorm clouds and fogs. Thunderclouds are not the only charged clouds in the atmosphere, and in fact other forms of clouds, especially extensive horizontal layer clouds (stratus), are much more abundant globally. Through developing new instrumentation carried on weather balloons, multiple soundings made in both hemispheres have confirmed that upper and lower boundary charging on extensive horizontal layer clouds occurs widely, likely to be a global phenomenon[2]. This is a result of the global atmospheric electric circuit, which links charge separation in thunderclouds with distant regions by current flowing throughout the atmosphere. The global circuit supplies the charge which accumulates on the upper and lower boundaries of layer clouds, and the upper boundaries of surface fogs.

The possible role of droplet charging in natural cloud processes has received relatively little attention. It has been suggested that the droplet charging influences the properties of the clouds, such as the stability of small droplets, the growth times from cloud droplets to raindrops by coalescence [3] and their reflection of sunlight [4], but this has hardly been investigated in natural water drop systems. To investigate the general possibilities around introducing artificially generated charge into natural droplet systems, real world experiments have been undertaken using corona ion emission into fogs, releasing from within [5] and above [6]. In this paper, the theory underlying the charging of the fog droplets is described (section 2), followed by the effect of charge on droplet evaporation (section 3). The design and implementation of the experiments is described in section 4, with the results obtained reviewed in section 5.

2. Droplet charging

In many atmospheric situations, electric fields present are small hence droplets charge by collection of diffusing cluster ions rather than ordered ion migration. The droplet charge can be calculated by evaluating the balance between the generation of positive and negative ions, and their loss by attachment to the droplets [7]. The theory describing this is now briefly summarised, and then used to represent (1) a typical natural fog situation, and (2) the situation when additional artificial ionisation is introduced.

2.1. Theoretical considerations

Charging on droplets can be evaluated by applying the principle of detailed balance [8,9]. If the positive and negative cluster ion concentrations are n_+ and n_- respectively, the variations with time t of the ion concentrations are given for positive ions by

$$\frac{dn_+}{dt} = q_+ - \alpha n_+ n_- - n_+ \sum_{j=-\infty}^{\infty} N_j \, \beta_{1,j} \tag{1}$$

and, for negative ions, by

$$\frac{dn_-}{dt} = q_- - \alpha n_+ n_- - n_- \sum_{j=-\infty}^{\infty} N_j \, \beta_{-1,j} \tag{2}.$$

In these equations the, q_+ and q_- represent positive and negative ion production rates respectively, and α is the ion-ion recombination coefficient. The last terms in each equation represent the loss rate of ions to the droplets. To evaluate this, there are assumed to be N_j droplets per unit volume of the same size, carrying j (integer) charges, and hence the summation is made across all possible values of charge. $\beta_{\pm 1,j}$ is the ion-droplet attachment coefficient, which quantifies the loss rate for ions of either polarity (± 1), to a droplet carrying j charges. For droplets carrying a charge j, their change in number concentration is given by an equation of the form

$$\frac{dN_j}{dt} = \beta_{1,j-1} n_+ N_{j-1} - \beta_{1,j} n_+ N_j + \beta_{-1,j+1} n_- N_{j+1} - \beta_{-1,j} n_- N_j \tag{3}.$$

A similar equation is required for each of the possible values of j, to represent all the charge categories which can occur. These equations couple the charge categories which are one charge unit greater or lesser, which a droplet will be transferred to through collision with a positive or negative ion. Using the analytical forms of the attachment coefficient ($\beta_{\pm 1,j}$) due to Gunn[10] which neglects image force attractions, Clement and Harrison[11] showed that, when the collision rates of ions and droplets became steady, the charge distribution on the monodisperse droplets was given by

$$\frac{N_j}{N_0} = \left[\frac{n_+ \mu_+}{n_- \mu_-}\right]^j \frac{8\pi\varepsilon_0 akT}{je^2} \, sinh\left[\frac{je^2}{8\pi\varepsilon_0 akT}\right] exp\left[\frac{-j^2 e^2}{8\pi\varepsilon_0 akT}\right] \tag{4},$$

with a mean charge j_m

$$j_m = \frac{4\pi\varepsilon_0 akT}{e^2} ln\left[\frac{n_+ \mu_+}{n_- \mu_-}\right] \tag{5}.$$

In these equations, a is the droplet radius, $\mu_\pm$ are the ion mobilities, k is Boltzmann's constant, T is the temperature, e is the modulus of the electronic charge and ε_0 is the permittivity of free space.

2.2. Charging under natural ionisation

An example of applying the set of coupled time-dependent equations (1) to (3) is given in figure 1, with the numerical solutions shown obtained using an adaptive step size Runge-Kutta method [12]. The

values for the droplet properties used are chosen for concentration and size to represent a stable natural fog. All droplets are assumed neutral initially, i.e. $N_0 = Z$ and $N_{j\neq 0} = 0$, where Z is the droplet number concentration. Equal ion production rates have been specified, with typical ion mobility values chosen for the near-surface atmosphere. In figure 1, (a) the ion concentrations increase steadily from initial conditions of zero, until steady-state values are reached due to ion-ion recombination and ion-droplet attachment, which are slightly different for positive and negative ions due to the asymmetry in their mobilities. The mean droplet charge (b) also becomes steady after the ion concentrations cease to change. (c) and (d) show samples from the evolution of the droplet charge distribution, which illustrate that it steadily broadens, as more and more droplets undergo ion collisions and acquire charges. The charge distribution in (d) shows good agreement with the analytical calculation from equation (4).

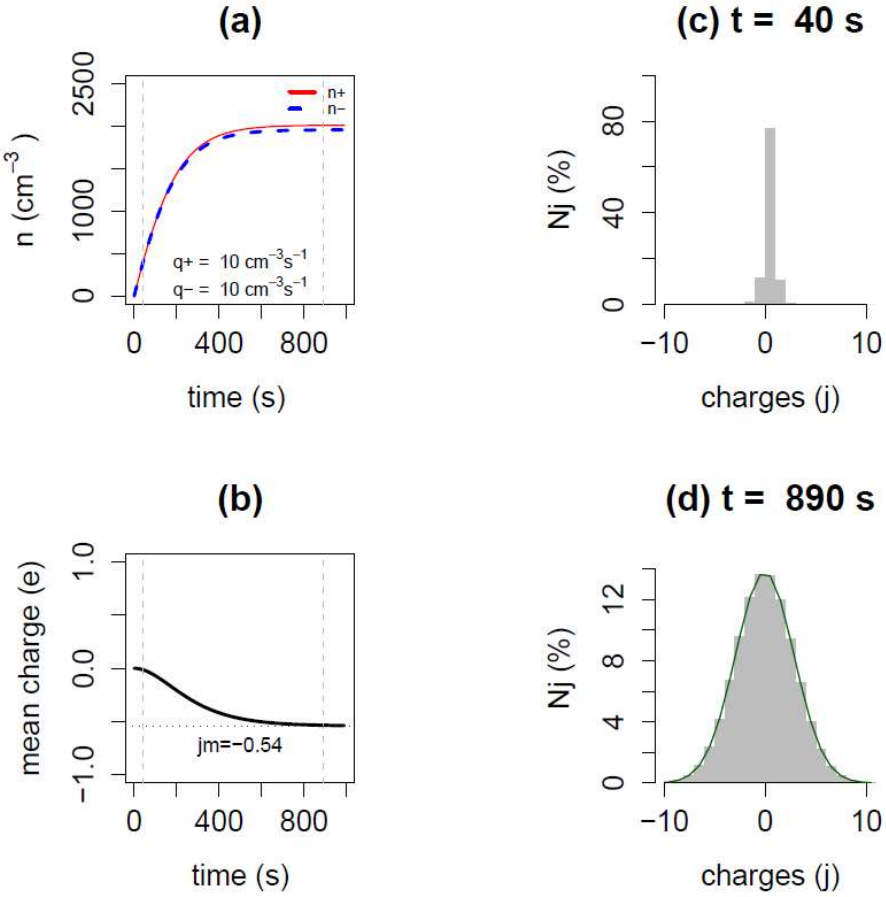

Figure 1. Evolution of charge on a system of 1 μm diameter droplets having 100 droplets cm^{-3}. (a) Variation of positive and negative ion concentrations with time, starting from zero initially, with q =10 cm^{-3} s^{-1}. (b) Mean charge obtained by summing across the entire droplet population at each time step. The horizontal dotted line shows the final mean charge j_m, calculated from equation (5). The two vertical lines indicate two instances chosen to produce (c) and (d), which show the droplet charge distributions at these times. In (d), the steady-state limit of the Modified Boltzmann Distribution (equation 4), has been added as a solid line. (Other parameters assumed: α=1.6×10^{-6} cm^3 s^{-1}, μ_+ = 1.14 cm^2 s^{-1} V^{-1}, μ_- =1.25 cm^2 s^{-1} V^{-1}, T = 5 °C).

2.3. Charging with artificial ionisation

If additional ionisation is introduced, for example by using a radioactive source or corona discharge, the ion production rates will be changed. Radioactivity will increase the ion production in a bipolar manner (yielding similar changes in q_+ and q_-), whereas corona will, in general, produce different

bipolar emission rates, i.e. $q_+ \neq q_-$. For a 1 μA corona current, the equivalent ion current is ~10^{13} s^{-1}, which, depending on the volume into which this disperses, would cause an ion production rate which is orders of magnitude greater than the natural near-surface value of ~10^7 m^{-3} s^{-1}.

Figure 2 shows the same system of equations used for figure 1, but with unequal ion production rates. For illustrative purposes, the negative ion production rate was 50× greater than that for the positive ions. In addition, the attachment coefficients used were those of Fuchs[13], as described in [8], which allow for image attractions between ions and droplets.

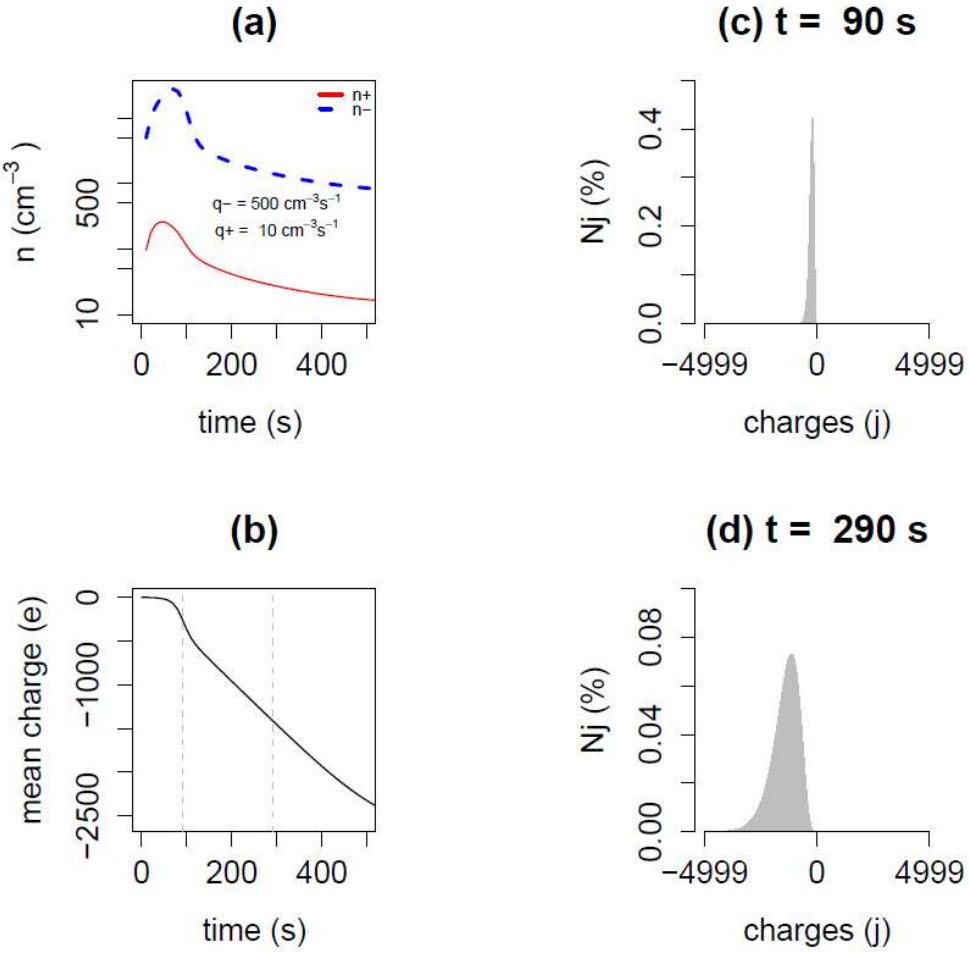

Figure 2. Evolution of droplet charge on the same system as for figure 1, but with different bipolar ion production rates ($q_\pm$ =10 cm^{-3} s^{-1} and q_- =500 cm^{-3} s^{-1}). (a) Variation of positive and negative ion concentrations with time. (b) Mean charge from summing across the entire droplet population. The two vertical lines indicate when (c) and (d) are obtained, which show the droplet charge distributions at these times.

These calculations indicate several consequences of $q_- \gg q_+$. Firstly, numerically, more charge categories are needed, as the magnitude of the droplet charge becomes much larger than in the natural fog charging case. This considerably slows the calculations. Secondly, the droplet charge generated is unipolar, dominated by negative charging from the negative ions. Thirdly, the charge distribution becomes skewed towards large negative charge values as time progresses. Fourthly, no final steady-state charge is reached, with the rate of increase of the mean charge between (c) and (d) ~ -5e per second. (This rate can also be estimated from $\frac{\Delta q}{Z}$, where $\Delta q = q_+ - q_-$). Overall, the effect of introducing the

unipolar ionizer is to steadily increase the droplet mean charge with the same polarity as the ions produced, and to steadily increase the small population of highly charged droplets.

3. Charging and evaporation

Whether water droplets grow or evaporate depends on the local water vapour concentration they encounter[14]. If the vapour pressure over the droplet surface is less than the local vapour pressure, the droplet grows, and if its surface vapour pressure exceeds the local vapour pressure, it will evaporate.

3.1. Evaporation equation

The variation in droplet radius a in response to local water vapour conditions is summarised by

$$a\frac{da}{dt} = \frac{D_v}{\rho_w R_v} f_V \left[\frac{e_\infty}{T_\infty} - f_T f_R \frac{e_s(T_a)}{T_a}\right] \quad (6),$$

which is equation (13-64) of [15]. The right-hand side term represents the difference between the ambient environment (with temperature T_∞ and vapour pressure e_∞) and the droplet (temperature T_a and surface vapour pressure e_s). The other terms are vapour diffusivity D_v, f_V a ventilation coefficient, the Rayleigh term f_R and Thomson term f_T. The Thomson and Rayleigh terms are given by

$$f_T = exp\left(\frac{2\gamma}{\rho_w R_v T_a a}\right) \quad (7)$$

and

$$f_R = exp\left(\frac{-j^2 e^2}{32\pi^2 \varepsilon_0 \rho_w R_v T_a a^4}\right) \quad (8)$$

respectively, with the additional terms introduced of the gas constant R_v, density ρ_w and surface tension γ.

The Rayleigh term provides the relationship between the droplet charge and physical behaviour. Using $f_R = f_T$, the *Rayleigh limit* can be found, which is the maximum charge a droplet of a specified size can sustain without disintegration. Alternatively, the *Rayleigh size* can be found, for a droplet carrying a specified charge. This is especially relevant when a charged droplet is evaporating, as it sets a minimum size at which a shrinking droplet will remain intact before electrical disintegration.

3.2. Charge effects on fog droplets

In a fog, the droplets present are in a saturated environment and therefore their size is generally stable. However, there will be fluctuations in the environmental conditions, leading to change in droplet size or the droplet may even evaporate. As is evident from equation (8), the effect of charge is greatest for small droplets. There may therefore be situations when, following environmental fluctuations, the survival or dissipation of a small droplet is influenced by the charge it carries.

An illustrative calculation of charge affecting droplet evaporation is given in figure 3. This was undertaken using equation (6), coupled with an additional equation (eqn 13-23 of [15]) to represent the droplet cooling during evaporation as

$$T_a = T_\infty + \frac{\rho_w L}{k_g} a\frac{da}{dt} \quad (9),$$

for k_g the thermal conductivity of the surroundings and L the latent heat of vaporisation. The evaporation considered was that of a 1 μm diameter droplet encountering slightly sub-saturated conditions (Relative Humidity = 99.9%), at 5 °C, Figure 3a shows that the evaporation process for such a droplet, which, when neutral, is found to have a duration of about 0.15 s.

The case of the same droplet being charged is now considered. Section 2 demonstrated that droplet charges of ~1000*e* can be generated using modest amounts of unipolar corona ionisation. Calculations

have therefore been made for a droplet carrying initial charges comparable with this, for example from the application of unipolar corona ionisation for tens of seconds. The charge obtained is assumed to be retained throughout the evaporation, and figure 3b shows the detail of the size changes at the smaller sizes shown. For droplet charges >1000*e*, the overall evaporation time is lengthened by the effects occurring at the smaller droplet sizes, in this example by 5 to 10%. Further, if the droplet charge is sufficient, the Rayleigh size may be reached as the droplet shrinks, and the evaporation will cease due to disintegration.

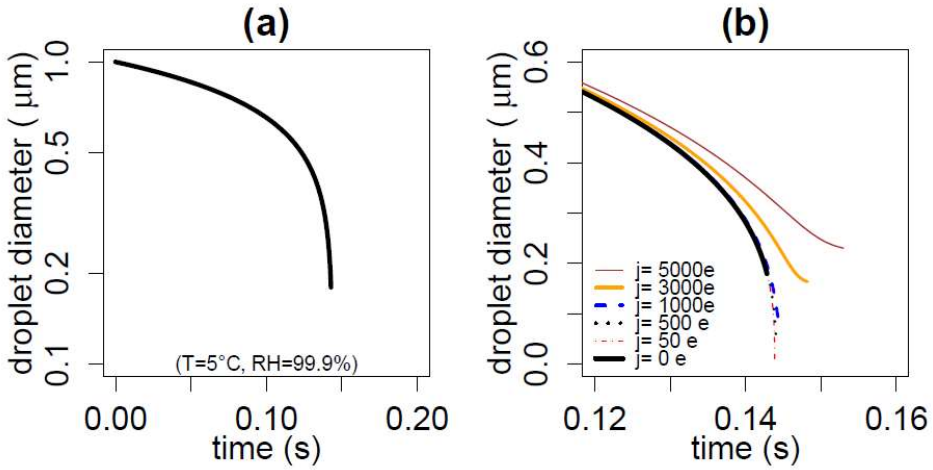

Figure 3. (a) Evaporation of a neutral 1 µm diameter droplet in air at 5°C and 99.9% Relative Humidity (RH). (b) Later stages of evaporation for a 1 µm diameter droplet carrying a range of initial charges j. (Constants: ρ_w =1000 kg m^{-3}, e = 1.6x10^{-19} C, ε_0=8.85x10^{-12} F m^{-1}, γ=7.2x10^{-2} N m^{-1}, R_v=461.5 J kg^{-1} K^{-1}, D_v = 2.91x10^{-5} m^2 s^{-1}, k_g=0.5918 W m^{-1} K^{-1}, L=2.26 MJ kg^{-1}. f_v =1 assumed).

4. Real world experiments

These indications from theory, that charge can influence the properties of small water droplets, have motivated experiments in natural fogs. These will be described in turn, firstly using a delivery system constructed for use within a surface fog, and secondly from above, by corona ion release from a specially designed remotely piloted aircraft.

4.1. Surface experiment

The University of Reading operates a farm at Sonning (51.48155 °N, 0.897154 °W), in the River Thames' flood plain, about 5 km from the main campus. This site was selected, as analysis of weather data from Sonning Farm showed that near-surface fogs typically occurred on several days annually.

Commercial and lab-constructed equipment was combined for this experimental work. The fog droplet size distribution was monitored with a Light Optical Aerosol Counter (LOAC) [16]. This draws air past a 25 mW 625 nm laser, generating a burst of scattered light from each droplet or aerosol particle, detected by two photodiodes, one of which is normal to the beam and the other at 60°. The optical pulse rate is proportional to the droplet concentration, and the two pulse heights related to the droplet size, providing, with processing, the droplet size distribution. The LOAC scans for 1 minute across 19 droplet size bins from 0.2 µm to 50 µm diameter, controlled by a Raspberry Pi (RPi) computer using USB data storage. In addition, the local atmospheric electric field was continuously sampled using a JCI131 electric field mill every second, mounted at 3 m height. At 3 m away, an array of four small negative corona emitters (Amazon type B01G1DA19O) were mounted at the top of a second mast. Figure 4 shows the arrangement used, with automatic switching and data logging.

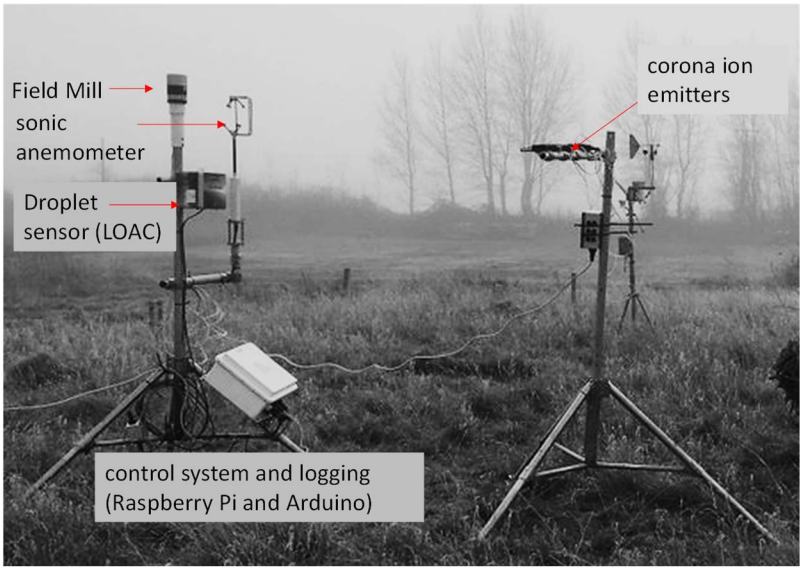

Figure 4. Arrangement of experimental apparatus at Sonning Farm, photographed in light fog. The left-hand mast carries a sonic anemometer, electric field mill, and the Light Optical Aerosol Counter (LOAC). The horizontal array of controlled corona emitters is on the right-hand mast. Adapted from [5]

The experimental procedure used in fog was to switch the unipolar corona emitters on and off every 10 mins, during which scans of the droplet sizes were made using the LOAC. The droplet size distributions obtained were divided into situations with and without the emitters on, and the data associated with each situation separately averaged together. Figure 5 shows the concentration data obtained from the sub-micron diameter droplets in (a) the emitter off cases and (b) the emitter on cases.

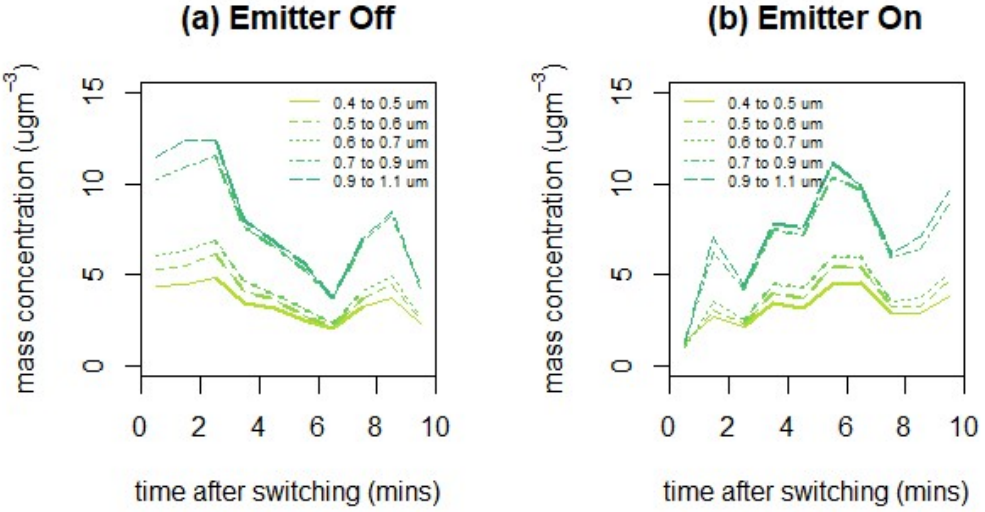

Figure 5. Concentrations of droplets recorded in the smaller (≤ 1 μm diameter) LOAC size bins during fog, averaged together during (a) emitter off (b) emitter on, for each minute after the switching transition. (The outer 2 mins of the composites are dotted due to timing uncertainty). Adapted from [5]

4.2. Aircraft experiment

In an alternative approach for charge delivery into fog, a specially instrumented Skywalker X8 aircraft (wingspan 2.1 m) was adapted to carry atmospheric sensors, with a negative ionizer under one wing and a positive ioniser beneath the other [17]. Even with small aircraft, experiments in fog are highly

challenging, as the aircraft deployment itself is difficult with limited visual range, and the equipment and staff need to be made ready rapidly whilst the fog persists.

A valley site was chosen for the experiments, where fog was reasonably common, near Castle Cary in the southwest of the UK (51.09788°N, 2.486905°W). When level flight was achieved, the ionisers were turned on and off in an identifiable sequence, as for the Sonning experiment, and the data in the different operating conditions grouped together to average the responses. Figure 6 summarises the aircraft trajectories used and presents data obtained from a photodiode sensor carried on the aircraft measuring the reflected sunlight from the fog beneath. Full details are given in [6]

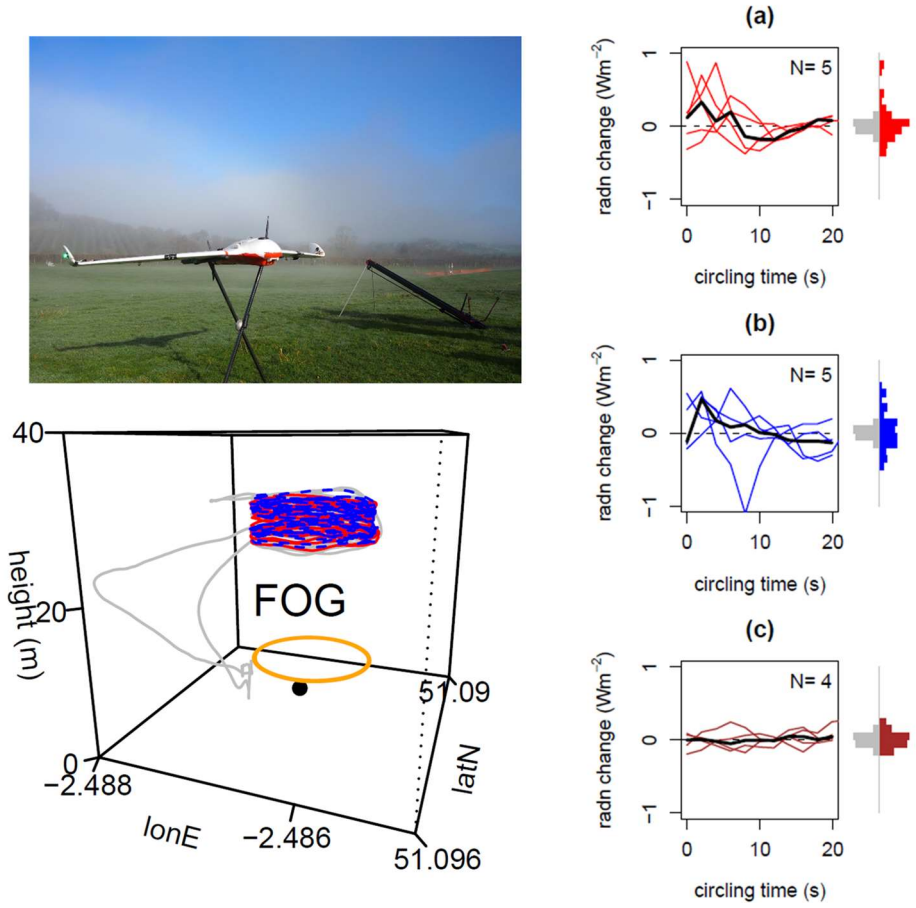

Figure 6. *(Left upper)* SkyWalker X8 aircraft before launch in fog, with catapult launcher (photo: Keri Nicoll). *(Left lower)* Trajectory of aircraft with repeated circular orbits above fog, with red and blue lines showing positive and negative ionisers on. *(Right panel)* Reflected solar radiation from fog, measured from aircraft (thin lines individual circles, thick line mean), for (a) positive ioniser on, (b) negative ioniser on and (c) both ionisers on. Adapted from [6]

5. Results

The two fog experiments used separate methodology, with different delivery and measurement systems. In the Sonning fog experiment, a tendency was apparent (figure 5) for the small droplet concentration to increase with the negative ion emitters operating. In the Castle Cary fog experiment (figure 6), greater reflectivity (~2%) from the fog occurred soon after the operation of the positive or negative ion emitters. These effects went away when both emitters were operating, when the net droplet charging would be expected to be much smaller than in either unipolar case.

6. Conclusions

Theory and numerical simulations indicate that corona ionization can generate substantial droplet charges in droplet systems typical of natural fogs, and that the droplet charging increases with the duration of the ionization. The charging is likely to be sufficient to influence the micron size droplets' physical behaviour. In natural world experiments it has been demonstrated that, during unipolar ion emission, changes occurred at the sub-micron end of the droplet size distribution. Fog reflectivity, which in general increases with an increase in the number of small droplets, also increased with unipolar ion emissions. This was not the case during bipolar ion emission. Taken together, these results support the possibility that natural droplet systems can be influenced by the introduction of charge.

Acknowledgments

This paper summarises collaborative work with contributions from University of Reading colleague Graeme Marlton and University of Bath collaborators Doug Tilley, Stefan Chindea, Pejman Iravani, Jonathan Du Bois, David Cleaver and Gavin Dingley. This work was supported by the National Center of Meteorology, Abu Dhabi, UAE under the UAE Research Program for Rain Enhancement Science (UAEREP).

References

[1] Schiffer M B 2003 *Draw the lightning down: Benjamin Franklin and electrical technology in the age of Enlightenment* (University of California Press)
[2] Nicoll K A and Harrison R G 2016 Stratiform cloud electrification: comparison of theory with multiple in-cloud measurements *Quarterly Journal of the Royal Meteorological Society* **142** 2679–91
[3] Ambaum M H P, Auerswald T, Eaves R and Harrison R G 2022 Enhanced attraction between drops carrying fluctuating charge distributions *Proceedings of the Royal Society A: Mathematical, Physical and Engineering Sciences* **478** 20210714
[4] Harrison R G, Nicoll K A and Ambaum M H P 2015 On the microphysical effects of observed cloud edge charging *Quarterly Journal of the Royal Meteorological Society* **141** 2690–9
[5] Harrison R G, Marlton G J, Ambaum M H P and Nicoll K A 2022 Modifying natural droplet systems by charge injection *Phys Rev Res* **4** L022050
[6] Harrison R G, Nicoll K A, Marlton G J, Tilley D J and Iravani P 2022 Ionic charge emission into fog from a remotely piloted aircraft *Geophys Res Lett* **49** e2022GL099827
[7] Harrison R G and Carslaw K S 2003 Ion-aerosol-cloud processes in the lower atmosphere *Reviews of Geophysics* **41** 1012
[8] Adachi M, Kousaka Y and Okuyama K 1985 Unipolar and bipolar diffusion charging of ultrafine aerosol particles *J Aerosol Sci* **16** 109–23
[9] Hoppel W A and Frick G M 1986 Ion—aerosol attachment coefficients and the steady-state charge distribution on aerosols in a bipolar ion environment *Aerosol Science and Technology* **5** 1–21
[10] Gunn R 1954 Diffusion charging of atmospheric droplets by ions, and the resulting combination coefficients *Journal of Meteorology* **11** 339–47
[11] Clement C F and Harrison R G 1991 Charge distributions on aerosols *Institute of Physics Conference Series 118* pp 275–80
[12] Press W H, Flannery B P, Teukolsky S A and Vetterling W T 1986 *Numerical Recipes in Pascal--The Art of Scientific Computing.* (Cambridge University Press)
[13] Fuchs N A 1963 On the stationary charge distribution on aerosol particles in a bipolar ionic atmosphere *Geofisica Pura e Applicata* **56** 185–93
[14] Ambaum M H P 2021 *Thermal physics of the atmosphere* (Amsterdam: Elsevier)
[15] Pruppacher H R, Klett J D and Wang P K 1998 *Microphysics of Clouds and Precipitation* (Dordrecht: Springer)

[16] Renard J B, Dulac F, Berthet G, Lurton T, Vignelles D, Jégou F, Tonnelier T, Jeannot M, Couté B, Akiki R, Verdier N, Mallet M, Gensdarmes F, Charpentier P, Mesmin S, Duverger V, Dupont J C, Elias T, Crenn V, Sciare J, Zieger P, Salter M, Roberts T, Gobbi M, Hamonou E, Olafsson H, Dagsson-Waldhauserova P, Camy-Peyret C, Mazel C, Décamps T, Piringer M, Surcin J and Daugeron D 2016 LOAC: A small aerosol optical counter/sizer for ground-based and balloon measurements of the size distribution and nature of atmospheric particles-Part 1: Principle of measurements and instrument evaluation *Atmos Meas Tech* **9** 3673–86

[17] Harrison R G, Nicoll K A, Tilley D J, Marlton G J, Chindea S, Dingley G P, Iravani P, Cleaver D J, Du Bois J L and Brus D 2021 Demonstration of a remotely piloted atmospheric measurement and charge release platform for geoengineering *J Atmos Ocean Technol* **38** 63–75